Corrosion Initiation Behavior of Thermal Control Oxidation Film of LA103Z Alloy

Chen Wen, Jingying Bai *, Kuo Zhao, Qingxin Cui, Baocheng Jiao, Xuguang Wang and Ligong Zhang

Beijing Spacecrafts, China Academy of Space Technology, Beijing, China

The magnesium lithium thermal control oxidation is a commonly used conductive anti-corrosion treatment method for aerospace. The corrosion behaviors of thermal control oxidation films for LA103Z alloys were studied in 3.5% NaCl solution. The corrosion characteristics with different immersion time were characterized by using scanning electron microscopy, energy spectroscopy, and electrochemical methods. The results showed that the corrosion of Mg-Li alloy with chemical oxidation film starts from pitting corrosion, gradually expands in depth in the early stage, forms corrosion holes, and then gradually develops into river-like morphology. In the last stage, the increasing corrosion products slow down the corrosion rate and gradually covers the entire sample surface. The corrosion product mainly consists of MgO, LiF, and $MgCl_2$. Combined with the electrochemical characteristics, the corrosion mechanism was investigated.

Keywords: corrosion, LA103Z, thermal control coating, electrochemical, electrochemical., initiation

INTRODUCTION

As the lightest metallic structural materials (1.30–1.65 g/cm^3), Mg-Li alloys have been widely used in space fields (Wu et al., 2020a; Wu et al., 2020b). In order to satisfy the functional requirements and adapt to the space environment, it needs to take out surface treatment such as plating, oxidation, and coatings for Mg-Li alloys (Xia et al., 2019; Zhang et al., 2019; Liu et al., 2021). However, due to the electrochemical activity of Mg and Li, the alloys have great corrosion risks in the service environment (Prando et al., 2019; Sun et al., 2020). Although there are few corrosive factors in space, the coastal launch site can bring severe corrosion for the products. Oxidation methods can form thermal control coatings, anti-corrosion coatings, coating suitable for bonding, etc., which are suitable for the structure applications of satellites (Shi et al., 2015; Guo et al., 2017; Yang et al., 2018; Qiu et al., 2020).

In order to improve cementing property, it is needed to reduce thickness of the coating; however, the thin coating is useless for preventing corrosion. Many researchers have made efforts to form thin coating with good corrosion resistance (Wang et al., 2007; Chen et al., 2011; Formosa et al., 2012; Fernández et al., 2019). Fernandez et al. (Fernández et al., 2019) found that reduced graphene oxide onto magnesium discs by electrochemical and chemical methods can decrease the corrosion rate. The results obtained by Chen et al. (Chen et al., 2011) indicated that all the conversion coating formed in different solutions exhibits amorphous structure. The formation of Mo on the surface of Mg alloys after chemical oxidation can significantly improve the corrosion resistance (Shao et al., 2017). Xu et al. (Xu et al., 2008) produced oxide film of 2–3 μm by the environment friendly chemical oxidation method. The corrosion resistance rate of the film in 3% NaCl solution was only 1/15 of Mg alloy substrates. Wang et al. (Liu et al., 2016) used black chemical oxidation to form a film, which had uniform blackness and dense film.

Element	Li	Al	Zn	Si	Fe	Mg
Content/%	10.0	3.2	2.8	0.05	0.05	Bal

In this paper, the thin film of magnesium lithium LA103Z was fabricated by chemical oxidation, and the corrosion behavior was studied by immersion test in 3.5wt% NaCl solution. The morphologies and corrosion products were characterized, combined with the electrochemical analysis of sample with different corrosion time, and the corrosion evolution mechanism was also studied.

EXPERIMENTAL SECTION

Experimental Sample and Procedure

The specimen used for the test is LA103Z magnesium lithium alloy, and the chemical composition is given in **Table 1**. The material was cut into 40 mm × 40 mm×2 mm for experiment. Moreover, the specimens were polished by sandpaper from 400#, 800#, to 1,000#.

Before oxidation, the specimens of LA103Z magnesium lithium alloy were degreased with absolute ethanol and then cleaned by deionized water → activation treatment by fluoride salt with concentration of 2.5 g/L → cleaned by deionized water → dried by compressed air. The chemical oxidation was carried out to obtain a thermal control film.

After oxidation, the specimens were sealed and protected by chloroprene rubber, except for an area of 40 mm × 40 mm for the immersion test. The specimens were soaked in 3.5% NaCl solution at the temperature 45°C with different times (1, 3, 6, 12, 18, 24 h). After immersion with the assumed time, the specimens were cleaned by deionized water and dried by compressed air. Specimens with different immersion time were cut off by cross-section and observed by SEM.

Characterization

After immersion test, the morphologies of the specimens were characterized by metallurgical microscope (MO, Canon E60) and scanning electron microscope (SEM, SUPRA55VPX,Germany). The composition of corrosion products was characterized by x-ray diffraction (XRD, Bruker AXS D8, Cu target, scan rate of 5°/min, scan range of 10°–90°).

The electrochemical evaluation with different immersion time was performed by using IM6 electrochemical equipment in 3.5wt % NaCl solution at room temperature. The experiment employed a three-electrode system, a saturated calomel (SCE) electrode as reference electrode, a Pt electrode as counter electrode, the magnesium lithium alloy chemical oxidation sample as working electrode, and the sample exposure area was $1 \, cm^2$. The open circle potential (OCP) was tested for 600 s. The electrochemical impedance spectroscopy (EIS) was tested with sinusoidal signal disturbance voltage amplitude of 10 mV. The frequency range is 100 kHz–10 mHz. The polarization curve test range is -0.5 V ~ +0.5 V (*vs* OCP), scan rate is 5 mV/s, the range of cyclic voltammetry test voltage is -0.25 V ~ +0.25 V (*vs* OCP), and the scan rate is 5 mV/s.

RESULTS AND DISCUSSION

Corrosion Morphologies

The morphology of the film and its element content are shown in **Figure 1**. The surface of the film contains many micro cracks and holes. The main elements are Mg, O, and Cr.

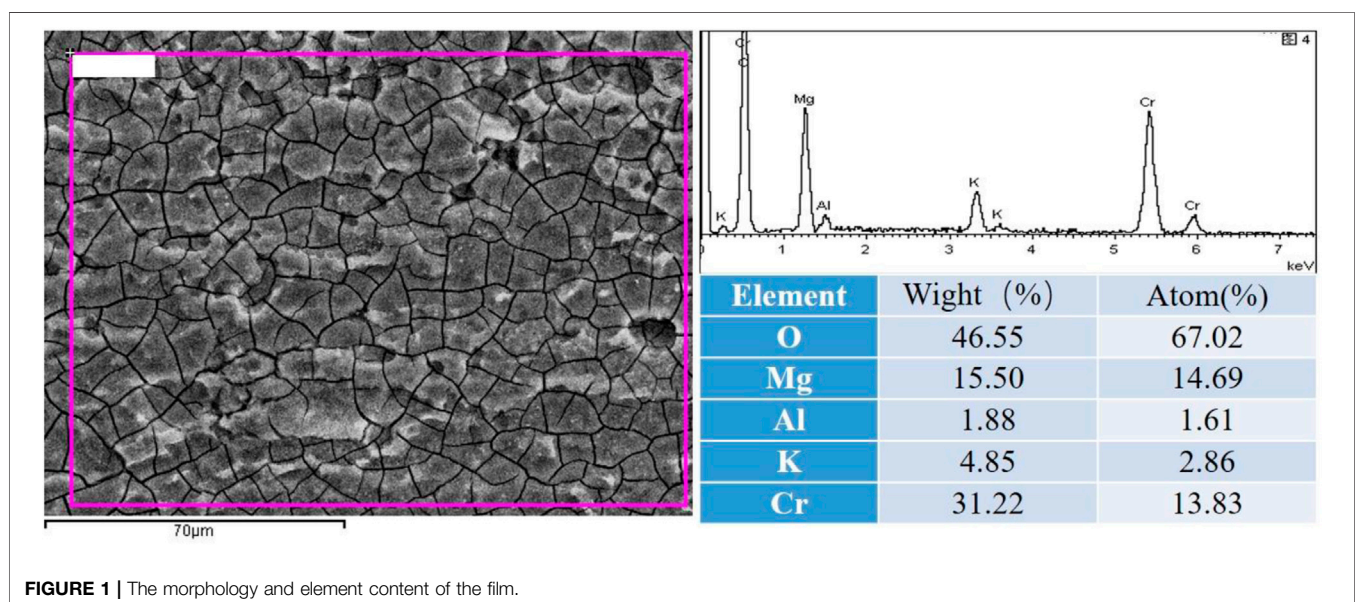| Element	Wight (%)	Atom(%)
O	46.55	67.02
Mg	15.50	14.69
Al	1.88	1.61
K	4.85	2.86
Cr	31.22	13.83

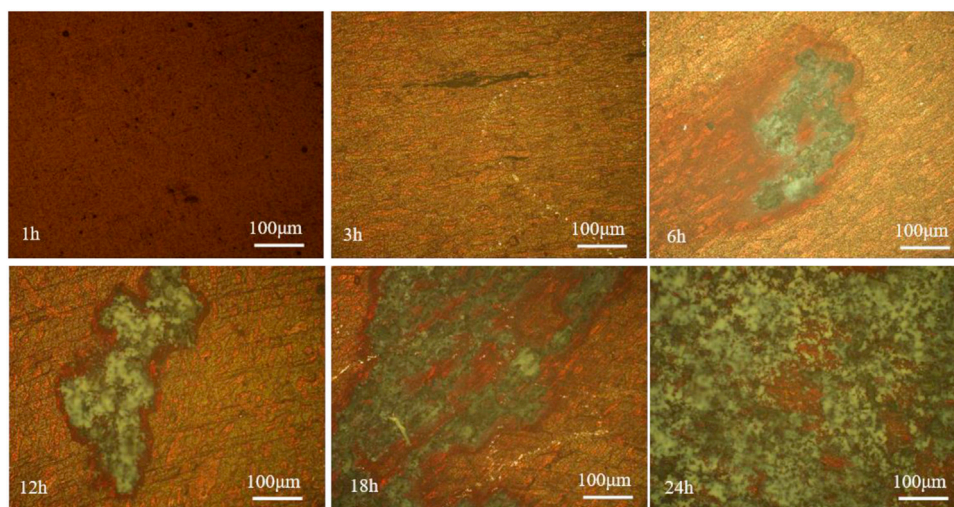FIGURE 1 | The morphology and element content of the film.

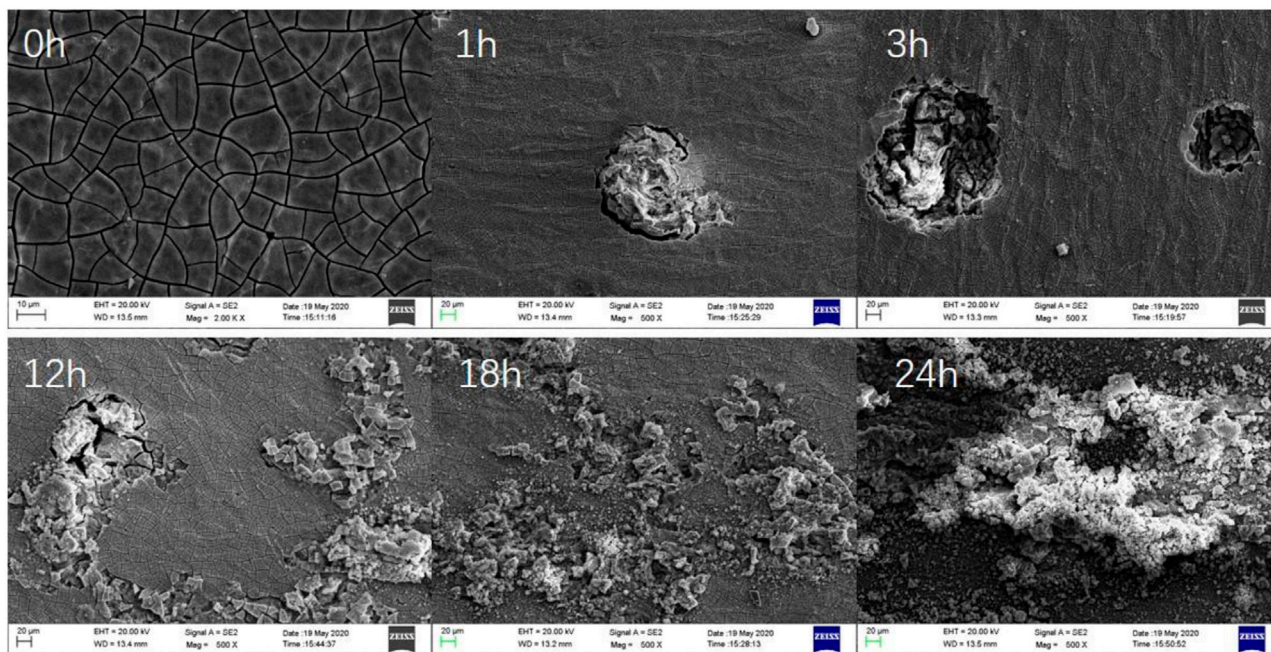FIGURE 2 | Surface morphologies of the specimens in 3.5% NaCl solution.

FIGURE 3 | SEM morphologies of the specimens in 3.5% NaCl solution.

The morphologies of the specimens after different immersion time are shown in **Figure 2**. It can be seen that when the specimens are immersed in NaCl solution, the surface forms black pits, which demonstrated that the pitting corrosion happens on the surface for 1 h. As the immersion time increases to 3 h, the surface is impregnated and the pits become dense, some of which develop to line. As the reaction continues, a big gray-green corrosion hole forms and gradually evolves into severe corrosion (6–12 h). The corrosion expands from the corrosion holes, which accelerates the corrosion, until the corrosion products almost cover the whole specimen surface (24 h).

In order to further study the evolution of the corrosion in NaCl solution, the micro morphologies after immersion for different time were characterized by SEM, which are shown in
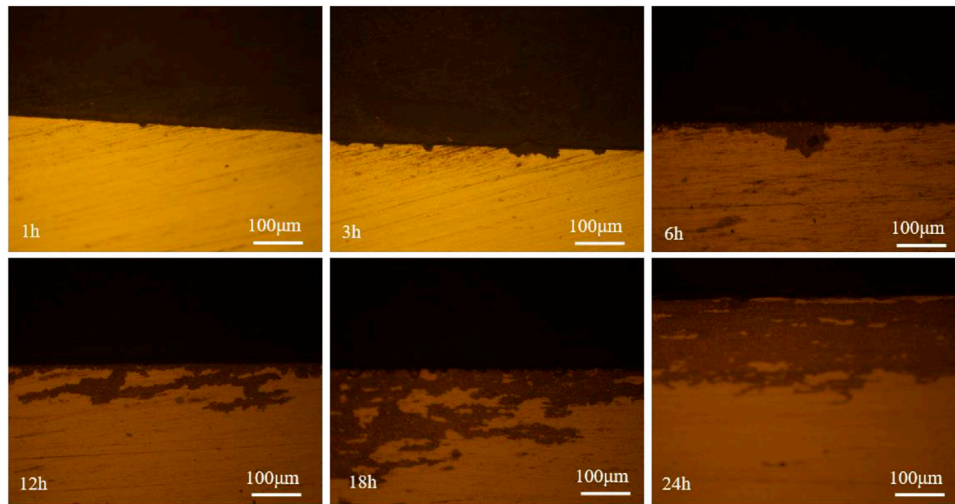
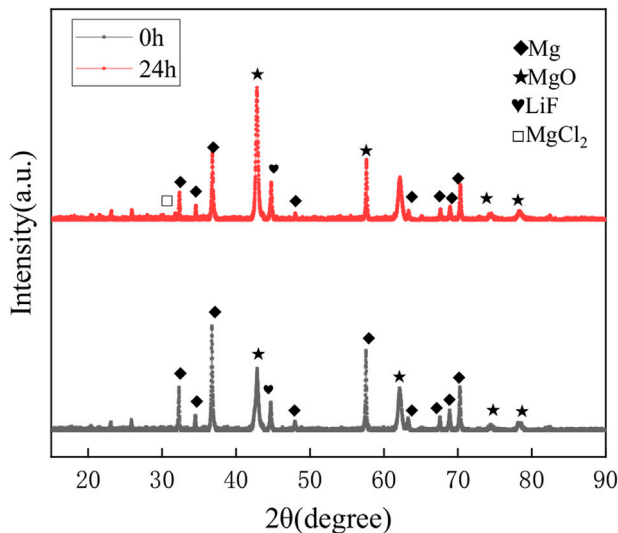**FIGURE 4 |** Cross-section morphologies of the specimens in 3.5% NaCl solution.

FIGURE 5 | XRD results of the specimens in 3.5% NaCl solution.

FIGURE 6 | Open circuit potential (OCP) plots of specimens with different immersion time.

Figure 3. After oxidation, the surface film is flat and locally covered with micro cracks. When immersed in the NaCl solution for 1 h, the electro active surface of the sample is dissolved and the corrosion products fall off, which promotes to the formation of pits. As the corrosion develops, the corrosion pit expands along the grain boundary (12 h) and the corrosion products present river-like morphology (12–18 h). As the corrosion exacerbates, fluffy corrosion products cover the surface of the sample.

The cross-section morphologies were characterized and shown in **Figure 4**. It can be seen that in the early stage of immersion (1 h), the corrosion is slight, and sporadic corrosion pits exist on the surface. Once the pit forms, the pits develop rapidly, which connect to form notch
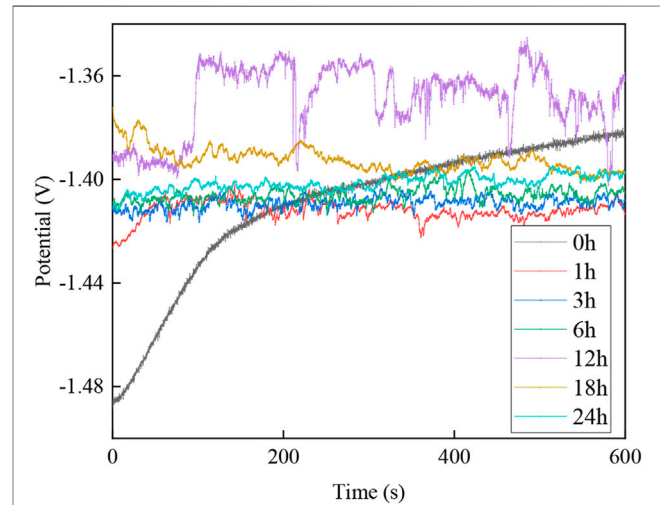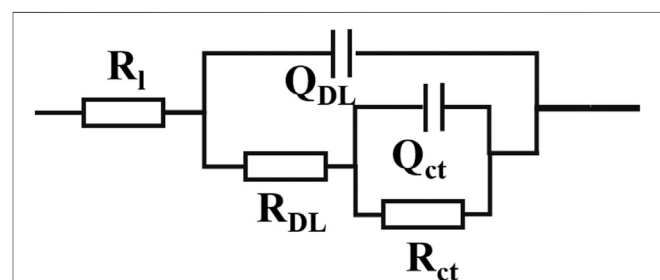

FIGURE 7 | Electrical equivalent circuit model for the EIS results, R (Q (R (QR))) (R$_l$ stands for solution resistance, Q$_{DL}$ and R$_{DL}$ are electric double layer capacitance and resistance respectively, Q$_{ct}$ and R$_{ct}$ are reaction capacitance and resistance respectively; Q is a constant phase angle element).
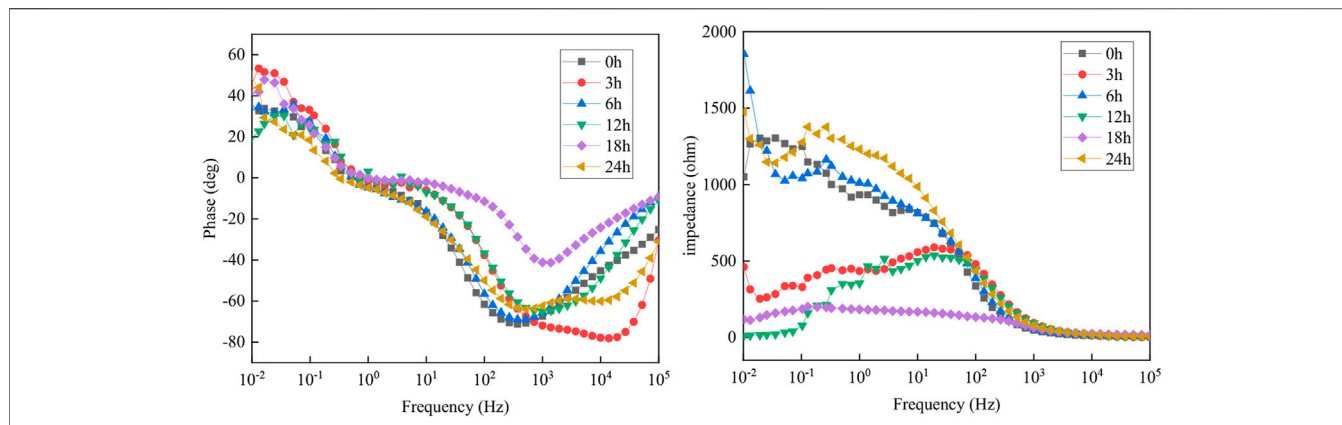
FIGURE 8 | EIS results of specimens after different immersion time.

TABLE 2 | Fitted data by Zsimpwin of EIS results.

Time (h)	R_I (ohm)	Q_{DL}		R_{DL}	Q_{ct}		R_{ct} (ohm)
		Y_{DL} (Ω^{-1} cm^{-2} s^{-n})	n		Y_{DL} (Ω^{-1} cm^{-2} s^{-n})	n	
0	13.02	4.129×10^{-6}	0.8907	947.8	7.660×10^{-6}	0.9453	1,050.5
3	10.72	6.858×10^{-6}	0.9324	664.1	4.393×10^{-6}	1	497.2
6	8.95	8.897×10^{-6}	0.9645	411.1	9.972×10^{-7}	1	475.7
12	15.91	2.608×10^{-6}	0.7756	334.1	7.106×10^{-7}	1	65.8
18	17.85	1.783×10^{-6}	0.7403	186.5	5.322×10^{-7}	1	103.6
24	22.37	1.282×10^{-6}	0.7193	122.6	2.628×10^{-7}	1	1,301.4

morphology. And the corrosion expands to depth direction, promoting the formation of corrosion holes. Based on the corrosion pits, the horizontal expansion of corrosion is obviously better than the vertical expansion, and finally a piece of corrosion morphology is formed, which gradually covers the entire sample surface.

The corrosion products were analyzed by XRD and the results are shown in **Figure 5**. It can be found that the oxidation film is consisted with MgO, LiF, and MgCl₂. As the corrosion happens, the diffraction peak intensity of MgO is much higher than that of Mg, which shows the opposite characters for 0 h, and the corrosion products contains MgCl₂, which indicates that Chloride ions participate in the reaction and promote the formation of corrosion products.

Electrochemical Results

The OCP results of the specimens after different immersion time are shown in **Figure 6**. After immersion, the potential of the sample quickly becomes positive and gradually stabilizes. With the immersion time increase, the open circuit potential becomes positive until 12 h and then gradually negative. It indicated that at the early stage (before 12 h), the corrosion product attaches to the surface and prevents the corrosion from developing, but as the immersion time goes on, the corrosion products become loose and blade off from the surface.
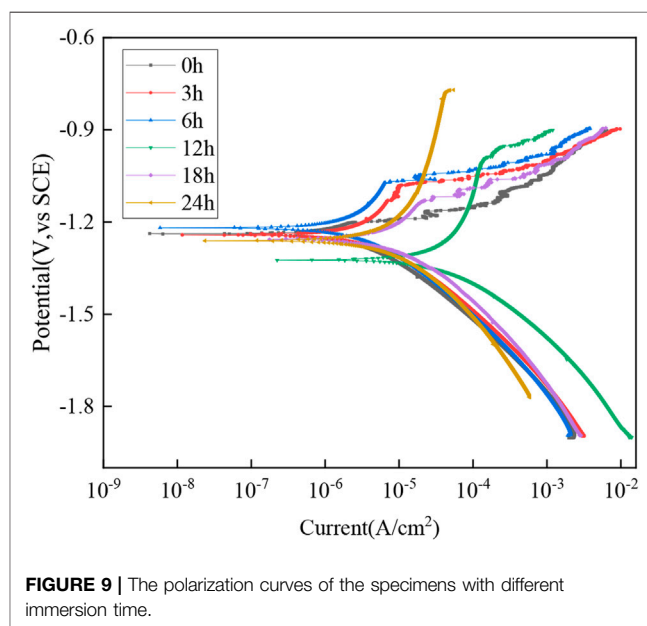

FIGURE 9 | The polarization curves of the specimens with different immersion time.

The structure of the electrochemical model of the specimens was characterized by EIS, and the fitting results for different immersion time of all specimens according to the electrical

TABLE 3 | The fitting calculation results for linear polarization zone of polarization curves.
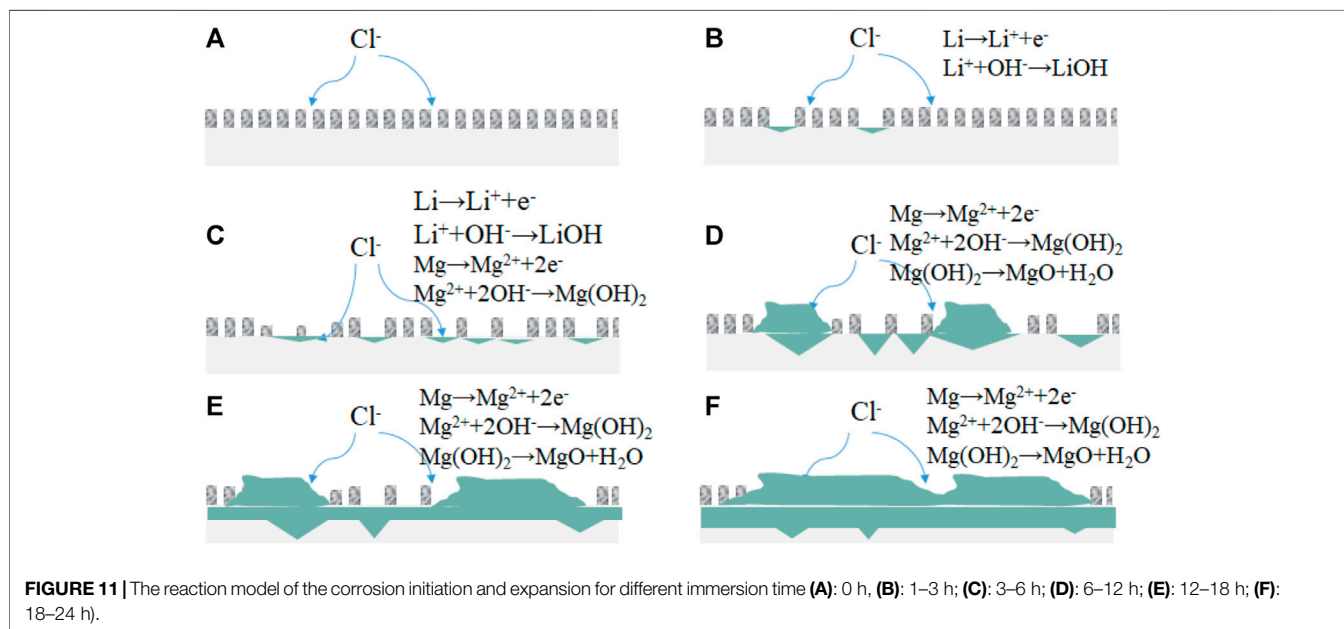
Time (h)	E_{corr} (V)	I_{corr} (A/cm²)	b_a (mV dec⁻¹)	b_c (mV dec⁻¹)
0	−1.255	2.435×10^{-6}	168.9	−132.1
3	−1.250	8.747×10^{-6}	67.5	−125.7
6	−1.232	9.238×10^{-6}	67.2	−124.5
12	−1.318	5.861×10^{-4}	38.6	−113.2
18	−1.247	1.103×10^{-5}	69.2	−111.7
24	−1.286	1.165×10^{-5}	75.3	−110.3

FIGURE 10 | The cyclic voltammetry curves after different immersion time.
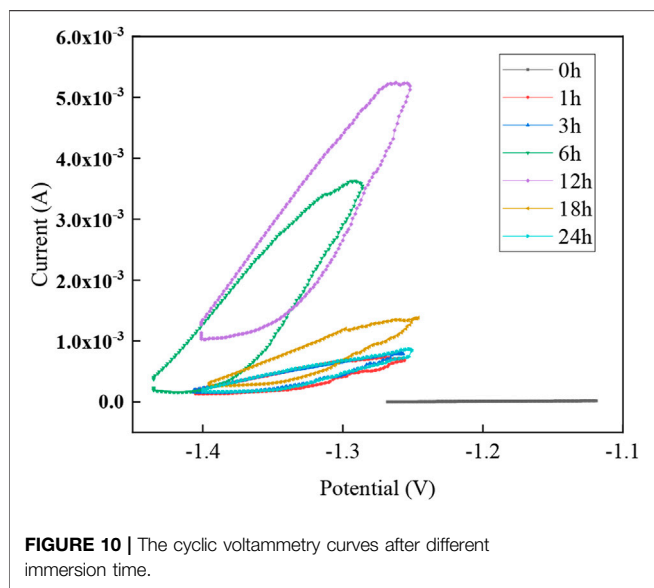
equivalent circuit model in **Figure 7** are shown in **Figure 8** and **Table 2**, respectively. From the Q_{ct} results can be seen that the capacitance value decreases from $7.660 \times 10^{-6} \, \Omega^{-1} \, cm^{-2} \, s^{-n}$ to $7.660 \times 10^{-6} \, \Omega^{-1} \, cm^{-2} \, s^{-n}$ as the immersion time increases from 0 to 24 h, which demonstrated that the resistance of corrosion product layer is reduced. However, although the reaction resistance is lower than that without immersion, as the immersion time increases from 1 h to 12 h, the reaction resistance decreases from 1,050.5 Ω to 65.8 Ω, indicating that the corrosion resistance of the sample decreases. From 12 to 24 h, the reaction resistance increases from 65.8 to 1,301.4 Ω. Combined with the morphologies, the corrosion happens when the specimens immersing in the NaCl solution and mainly forms pits and holes before 12 h, and then the corrosion products formed on the surface for 12–24 h, which has a certain blocking effect in the film layer, and the corrosion rate decreases.

The polarization plots after different immersion time are shown in **Figure 9**. The self-corrosion potential and self-corrosion current obtained by the linear fitting for polarization zone are given in **Table 3**. Compared with the non-immersed sample, the immersed sample has a smaller corrosion current and higher corrosion resistance, which indicates that the immersion reduced the corrosion resistance of the film. The self-corrosion potential shows the same trend with the open circuit potential. From the self-corrosion, current data show that the current increases from 2.435×10^{-6} A/cm² to 5.861×10^{-4} A/cm² before 12 h, which indicates that the corrosion reaction is exacerbated, consistent with the reaction resistance. However, as the corrosion products cover the reaction area (anodic zone), which prevents the corrosion, the anodic resistance (b_a) of the specimen increases after 12 h. However, the cathode area is still exposed to the solution and the continuous reaction leads to a decrease in cathode reaction resistance (b_c) from 132.1 mV dec⁻¹ to 110.3 mV dec⁻¹ with the increasing time from 0 to 24 h.

FIGURE 11 | The reaction model of the corrosion initiation and expansion for different immersion time **(A)**: 0 h, **(B)**: 1–3 h; **(C)**: 3–6 h; **(D)**: 6–12 h; **(E)**: 12–18 h; **(F)**: 18–24 h).

The cyclic voltammetry curves after different immersion time are shown in **Figure 10**. It can be seen that the current response to voltage change of the specimens without immersion is the smallest and basically presents a reversible process, which indicates that the sample has good corrosion resistance. The corrosion processes are shown in **Figure 11**. As the reaction time increases from 0 to 12 h, the current response is more obvious and the degree of reversibility gets lower and lower, which demonstrates that the electrochemical reaction is more and more violent. But the irreversible process of the reaction weakens from 12 to 24 h, which is caused by the corrosion products.

Discussion

From the corrosion morphologies, composition of the corrosion products, and the electrochemical results, the process of corrosion initiation and development is given as **Figure 10**. The corrosion process can be concluded into the following processes.

The initial stage of corrosion initiation (a-b) is mainly the formation of pits due to the electrochemical solution of Li, as it is the most electrochemically active element. When the immersion continues, the element Mg happens in corrosion, and Li reacts further and dissolves off, which leads to the pits expanding to corrosion holes (b-c), and corrosion rate increasing as the corrosion products accumulate on the surface of the specimen (c-d), the micro-electro-battery and dissolution effect are more obvious, and the corrosion is further intensified, and corrosion develops mainly towards horizontal (d-e). However, after the corrosion products cover most of the surface, the micro-battery effect reduces, and the horizontal reaction slows down. And the corrosion products on the surface changes from $Mg(OH)_2$ to MgO, which is more loose than $Mg(OH)_2$, leading to depth corrosion acceleration.

The wedge effect of corrosion products leads to thickening of corrosion products.

CONCLUSION

1) The corrosion of Mg-Li alloy with chemical oxidation film starts from pitting corrosion, gradually expands in depth in the early stage, forms corrosion holes, and then gradually develops into river-like morphology. In the last stage, the increasing corrosion products slow down the corrosion rate and gradually cover the entire sample surface.
2) The corrosion product is mainly consisted with MgO, LiF, and $MgCl_2$.
3) The initial stage of corrosion initiation is mainly the formation of pits due to the electrochemical solution of Li. When the immersion continues, the element Mg happens as corrosion, and Li reacts further and dissolves off, leading to the pits expanding to corrosion holes. As the corrosion products accumulate on the surface of the specimen, the micro-electro-battery and dissolution effect are more obvious, and the corrosion is further intensified, and corrosion develops mainly towards horizontal.

DATA AVAILABILITY STATEMENT

The raw data supporting the conclusions of this article will be made available by the authors, without undue reservation.

AUTHOR CONTRIBUTIONS

All authors listed have made a substantial, direct, and intellectual contribution to the work and approved it for publication.

REFERENCES

Chen, D. C., Wu, J. F., Liang, Y. Q., Ye, S. L., and Li, W. F. (2011). Preparation and Elements Analysis of Porous Fluorescent Glasses. *Trans. Nonferrous Met. Soc. China.* 21, 1905–1910. doi:10.1016/s1003-6326(11)60948-5

Fernández, J., El Ouardi, Y., Bonastre, J., Molina, J. M., and Cases, F. (2019). Modification of the Magnesium Corrosion Rate in Physiological saline 0.9 Wt % NaCl via Chemical and Electrochemical Coating of Reduced Graphene Oxide. *Corros. Sci.* 152, 75–81. doi:10.1016/j.corsci.2019.01.025

Formosa, J., Chimenos, J. M., Lacasta, A. M., and Niubo, M. (2012). Interaction between Low-Grade Magnesium Oxide and Boric Acid in Chemically Bonded Phosphate Ceramics Formulation. *Ceram. Int.* 38, 2483–2493. doi:10.1016/j.ceramint.2011.11.017

Guo, L., Zhang, F., Song, L., Zeng, R.-C., Li, S.-Q., and Han, E.-H. (2017). Corrosion Resistance of Ceria/polymethyltrimethoxysilane Modified Magnesium Hydroxide Coating on AZ31 Magnesium alloy. *Surf. Coat. Tech.* 328, 121–133. doi:10.1016/j.surfcoat.2017.08.039

Liu, R., Liu, Z. H., Wang, F., Jia, Y. F., Ding, Y. D., Ban, G. D., et al. (2016). Development of Corrosion Surface Modification Technology for Magnesium Alloys. *Mater. Protect.* 45 (4), 124–133. doi:10.16490/j.cnki.issn.1001-3660.2016.04.021

Liu, S., Qi, Y., Peng, Z., and Liang, J. (2021). A Chemical-free Sealing Method for Micro-arc Oxidation Coatings on AZ31 Mg alloy. *Surf. Coat. Tech.* 406, 126655–126665. doi:10.1016/j.surfcoat.2020.126655

Prando, D., Nicolis, D., Bolzoni, F., Pedeferri, M., and Ormellese, M. (2019). Chemical Oxidation as Repairing Technique to Restore Corrosion Resistance on Damaged Anodized Titanium. *Surf. Coat. Tech.* 364, 225–230. doi:10.1016/j.surfcoat.2019.03.005

Qiu, Z.-m., Zeng, R.-c., Zhang, F., Song, L., and Li, S.-q. (2020). Corrosion Resistance of Mg−Al LDH/Mg(OH)2/silane−Ce Hybrid Coating on Magnesium alloy AZ31. *Trans. Nonferrous Met. Soc. China* 30, 2967–2979. doi:10.1016/s1003-6326(20)65435-8

Shao, Z., Zhang, F., and Zhang, Q. (2017). Preparation of Grayish Black Film on Am50 Magnesium Alloy by Chemical Conversion–Micro-Arc Oxidation. *Surf. Rev. Lett.* 24 (1), 1750012–1750019. doi:10.1142/s0218625x17500123

Shi, P., Niu, B., and Li, Q. (2015). Preparation and Characterization of PLA Coating and PLA/MAO Composite Coatings on AZ31 Magnesium alloy for Improvement of Corrosion Resistance. *Surf. Coat. Tech.* 262, 26–32. doi:10.1016/j.surfcoat.2014.11.069

Sun, Y., Wang, R., Peng, C., and Cai, Z. (2020). Microstructure and Corrosion Behavior of As-Extruded Mg-xLi-3Al-2Zn-0.2Zr Alloys (X = 5, 8, 11 wt.%). *Corrosion Sci.* 167, 108487–108501. doi:10.1016/j.corsci.2020.108487

Wang, W., Qiao, X. L., Chen, J. G., and Li, H. J. (2007). Facile Synthesis of Magnesium Oxide Nanoplates via Chemical Precipitation. *Mater. Lett.* 61, 3218–3220. doi:10.1016/j.matlet.2006.11.071

Wu, G., Zhao, D., Lin, X., Liu, J., and Ji, X. (2020). Investigation of an Environmentally Friendly Coloring Coating for Magnesium-Lithium alloy Micro-arc Oxidation. *Surf. Inter.* 20, 100513–100518. doi:10.1016/j.surfin.2020.100513

Wu, G., Zhao, D., and Sun, L. (2020). Microstructure and Mechanical Properties of Wire-Filled Tungsten Argon Arc Welded Joints for LA141 Magnesium-Lithium-Aluminum alloy. *Mater. Today Commun.* 23, 100881–100886. doi:10.1016/j.mtcomm.2019.100881

Xia, Q., Zhang, D., Li, D., Jiang, Z., and Yao, Z. (2019). Preparation of the Plasma Electrolytic Oxidation Coating on Mg Li alloy and its thermal Control Performance. *Surf. Coat. Tech.* 369, 252–256. doi:10.1016/j.surfcoat.2019.04.073

Xu, H., Wang, Q., and Zhang, Z. (2008). *Mater. Prot.* 41 (9), 20–23.

Yang, W., Xu, D., Wang, J., Yao, X., and Chen, J. (2018). Microstructure and Corrosion Resistance of Micro Arc Oxidation Plus Electrostatic Powder Spraying Composite Coating on Magnesium alloy. *Corrosion Sci.* 136, 174–179. doi:10.1016/j.corsci.2018.03.004

Zhang, Y., Chen, F., Zhang, Y., Liu, Z., Wang, X., and Du, C. (2019). Influence of Graphene Oxide on the Antiwear and Antifriction Performance of MAO Coating Fabricated on Mg Li alloy. *Surf. Coat. Tech.* 364, 144–156. doi:10.1016/j.surfcoat.2019.01.103